Polymer 51 (2010) 1728–1736

Contents lists available at ScienceDirect

Polymer

journal homepage: www.elsevier.com/locate/polymer

Polypyrrole nanocoatings of poly(styrene-*co*-methacrylic acid) particles

M.I. Redondo [a,*], M.V. García [a], E. Sánchez de la Blanca [a], M. Pablos [a], I. Carrillo [b], M.J. González-Tejera [a], E. Enciso [a]

[a] Dpt. Química Física I, Fac. Ciencias Químicas, Univ. Complutense, 28040-Madrid. Spain
[b] Dpt. Química Industrial y Polímeros, E.U.I.T. Industrial, Univ. Politécnica de Madrid, 28012-Madrid, Spain

ARTICLE INFO

Article history:
Received 28 September 2009
Received in revised form
10 February 2010
Accepted 15 February 2010
Available online 21 February 2010

Keywords:
Latex templates
Polypyrrole nanocoating
Percolation

ABSTRACT

In this study the properties of polypyrrole (PPy) nanocoating over poly(styrene-*co*-methacrylic acid) (PS-MAA) particles were investigated. Monodisperse PS-MAA templates were obtained by free surfactant emulsion polymerization. The addition of methacrylic acid into the monomer feed mixture reduced particle size, ionic charge and hydrophobicity of the template surface. Correlations between template sizes and compositions, PPy confinement (granularity, shell size, etc.) and electrical conductivity, σ, are discussed. After dissolving the PPy/PS-MAA composites in tetrahydrofurane, PPy void spheres are obtained proving the core-shell nature of the coated particles. Bare styrene templates show densely packed PPy coatings and electrical conductivities near 7 S cm^{-1} at high PPy loadings; on the contrary, at the same PPy mass percentage, the richer methacrylic acid particles show low packed PPy grains and conductivities that fall to 0.8 S cm^{-1}. In core-shell particles the PPy mass per unit area, Γ, is the key parameter which determines the insulator–conductor transition for any particle size. The conductivity values of PPy/PS-MAA composites follow a percolation law: $\sigma \propto (\Gamma - \Gamma_c)^t$, with a critical threshold $\Gamma_c = (0.262 \pm 0.002) \times 10^{-6}$ g cm^{-2}. The critical exponent obtained $t = 1.98 \pm 0.07$ agrees with the predicted value $t = 2.0$ for three-dimensional lattices of random resistors.

1. Introduction

The interest in conducting polymers (CP) on both scientific and technological application levels has been continuously increasing in the last decades [1]. Polypyrrole (PPy) is one of the most studied CP owing to its easy electrochemical and chemical synthesis [2,3], high electrical conductivity and environmental stability. However the low PPy solubility makes its processability difficult and so many efforts to improve it have been made. Coating of latex particles has been proposed to obtain processable polypyrrole both by electrochemical [4,5] or chemical pyrrole polymerization in the presence of different latexes [6–15].

Many of the published studies are referred to PPy coated polystyrene (PS) latexes. For instance, Armes and co-workers have extensively investigated the colloid stability, conductivity, morphology and surface composition of micrometer-sized PPy coated polystyrene latexes [8–10]. They used poly(*N*-vinylpyrrolidone) (PVP) as stabilizer and found that if the PPy overlayer was thin enough, the resulting colloid was moderately stable. Depending on synthesis conditions, conductivity values up to 6 S cm^{-1} were measured [9]. A core-shell morphology was proved [10] for those composites. In contrast, PPy coated submicrometer-sized poly (ethylene glycol)-stabilized PS latexes did not present a core-shell morphology [11] and their conductivity values were about 10^{-2} S cm^{-1}. Recently Lu [16] and co-workers published a detailed study on the influence of pyrrole loading, overall template surface area and of polypyrrole polymerization kinetics, over the electrical conductivity of PPy coated poly(styrene co-ethylene glycol) methacrylate particles. However, few data have been reported so far on the relationship between surface chemical composition, particle diameter, morphological aspects of the PPy coatings and the electrical conductivity.

The aim of this paper is the synthesis and characterization of PPy-coated monodisperse submicrometer latexes of styrene, copolymerized with methacrylic acid (MAA) moieties. We focus on the influence of methacrylic acid concentration and PPy loading on particle morphology and conductivity. The two steps of the synthesis: (a) preparation of monodisperse poly(styrene-*co*-methacrylic acid) (PS-MAA) spheres, with appropriate MAA surface loading and controlled particle size and (b) deposition of PPy by chemical oxidative polymerization process are also discussed. Finally, the insulator–conductor transition of these composites is analyzed in terms of the PPy loading mass per latex unit area.

* Corresponding author. Tel.: +34 913944277; fax: +34 913944135.
E-mail address: iredondo@quim.ucm.es (M.I. Redondo).

0032-3861/$ – see front matter © 2010 Elsevier Ltd. All rights reserved.
doi:10.1016/j.polymer.2010.02.027

2. Experimental section

2.1. Materials

Styrene (S), methacrylic acid (MAA) (reagent grade), potassium persulphate (KPS) initiator and $FeCl_3 \cdot 6H_2O$ (Sigma, >98%) from Sigma–Aldrich were used as received. Pyrrole from Across Organic (99% purity) was vacuum distilled before use. All the solutions were prepared with distilled water (Milli-Q).

2.2. Synthesis of PS-MAA particles

Spherical particles of PS-MAA latexes were prepared from surfactant-free emulsion by a standard copolymerization process of styrene and methacrylic acid [17,18] at different MAA/total monomer weight percentage: 0, 0.5, 1.4, 3.2 and 7.4 (samples 1, 2, 3, 4, 5 hereafter). The polymerization reactions have been carried out in a 500 mL round-bottomed, four-necked flask. In one of the outlets, a T-shaped stirrer was inserted. In another neck, a water-cooled reflux condenser was fitted. A third outlet was equipped with a gas inlet. The last one was closed and used to introduce chemicals. The flask was put into a thermostat water bath which controlled the reaction temperature to ±2 °C. A typical reaction, corresponding with the preparation of sample 3 particles, follows these steps: 228 mL of distilled water are introduced in the flask together with the monomer mixture: 31 g of styrene and 0.45 g of MAA. Styrene was washed three times with NaOH 0.1 M water solution and two times with distilled water to eliminate the monomer inhibitor. The flask is then heated to 68 °C. Stirring is adjusted to 350 rpm and nitrogen gas is bubbled through the mixture to remove the oxygen from the system. Then, 0.3 g of KPS solved in 7 mL of distilled water was added. After 18 h of reaction time, the flask is removed from the bath and cooled in a water-ice mixture. A sample of 2–3 mL is oven-dried at 50 °C to obtain the polymerization reaction yield. The resulting latex is filtered with wool glass and dialyzed against water over three weeks.

2.3. Preparation of PPy coated PS-MAA latexes

Polypyrrole was synthesized and deposited onto latex particles following the chemical method proposed by Perruchot et al. [8]: 0.23 g (series A), 0.46 g (series B) or 0.79 g (series C) of $FeCl_3 \cdot 6H_2O$ were solved in 15 mL of the corresponding PS-MAA latex aqueous dispersion (2 wt% of solid content). Afterwards a pyrrole (Py) volume of 0.025 mL, 0.050 mL or 0.075 mL (series A, B, C, respectively) was added. The reactive amounts were calculated to give theoretical PPy loadings (weight% PPy/latex) of about 8%, 16% and 24% in series A, B and C respectively, assuming the reaction stoichiometry proposed by Armes et al. [19]. The reaction began immediately as indicated by the color change. After 1 h stirring the polymerization reaction was allowed to continue for about 24 h. The dark dispersions were centrifuged and the supernatant liquid decanted. The solid sediments were redispersed in deionized water. The last step was repeated three times to eliminate any byproducts. After synthesis PPy/PS-MAA composites were oven dried at reduced pressure at 50–60 °C for about 20 h. Throughout this paper these coated latex are identified by a number (from 1 to 5) indicating the kind of latex and a letter (A, B, C) for the PPy loading.

2.4. Particles characterization

Scanning electron microscopy (SEM) to analyze the surface morphology of PS-MAA and PPy/PS-MAA latexes was performed with a JEOL-JSM-6330F Electron Microscope operating at 10 kV. To prevent charge built up, the samples were prepared by sputtering a thin gold film over a small amount of dried particles placed into an appropriate support. No metallization effects over morphology were detected.

The size of the particles was evaluated using the line start mode of a disk centrifuge photosedimentometer (DCP) (Brookhaven BI-DCP), and by measuring several arrays of particles, involving 20–30 particles, in the SEM pictures. Electrophoretic mobility was determined with a Zeta Sizer Nano ZS, Malvern instrument using in each case three dilute samples (0.024 wt% solid content) at a temperature of 25 °C and a ionic strength of 1 mM KNO_3. The tests of latex stability have been performed by adding NaCl solutions to 0.1 wt% and 0.5 wt% latex suspensions. In a vial, 1 mL of latex suspension was mixed with 1 mL of electrolyte solution in the concentration range 0.1–0.4 M. After 24 h the stability of the suspension was checked by eye inspection. Three independent tests were performed to obtain an average critical coagulation concentration (*ccc*).

Actual PPy loading was determined by elemental analysis using a microanalyzer LECO CHNS-932. PPy coatings thickness was estimated by transmission electron microscopy (TEM) using a JEOL-JEM-2000FX Electron Microscope operating at 200 kV. The hollow PPy spheres obtained after solving latex cores in tetrahydrofurane, were dispersed in buthyl alcohol.

Chemical structure of PPy coated PS-MAA samples was confirmed by FTIR spectra recorded at a resolution of 4 cm^{-1} in a Perkin–Elmer Spectrum 100 FTIR instrument. Samples were prepared as KBr pellets (0.25 mg of PPy/PS-MAA were dispersed in 300 mg of KBr in all cases).

2.5. Conductivity measurements

Conductivity measurements were carried out on 25 mg dried sample pellets (1.2 cm diameter) pressed at 3 Tm. SEM images indicated that particle deformation was not very important at this pressure. A standard four point probe method was used to determine the sample DC conductivity at room temperature using a Keithley Model 2000 multimeter. The error was estimated to be in the range 15–20%.

3. Results and discussion

3.1. PS-MAA particles

The synthesized particles were spherical with a smooth surface morphology. When the suspension was dried the particles self assemble into nice face centered cubic crystals, as it corresponds to high packed monodisperse spheres (Fig. 1). The high solubility and reactivity of the MAA monomer in the aqueous phase enhances the rate and yield of the polymerization (see Table 1).

The introduction of MAA monomer inside the particles was followed by infrared spectroscopy. FTIR spectra of studied samples in the ν (C=O) (1700 cm^{-1}) and ν (C=C) (1600 cm^{-1}) region are depicted in Fig. 2a. A linear relationship between Abs_{1700}/Abs_{1600} and wt% MAA/monomer is also shown (Fig. 2b). The observed correlation shows that the MAA content inside the latex particles mirrors the MAA amount in the feed mixture. As can be observed in Fig. 2b, the absorbance ratio is zero at a very low (but no null) value of MAA concentration, which indicates that a small amount of MAA has not polymerized within the latex particles. This MAA remains in solution as small soluble chains, raising the osmotic pressure of the suspension. This justifies the observation that latexes with large MAA loadings show large increments of suspension volume during the dialysis.

The amount of styrene monomer and KPS initiator in the feed were fixed for all samples. Therefore the origin of the particle size reduction shown in Table 1 must be the presence of hydrophilic co-monomer.

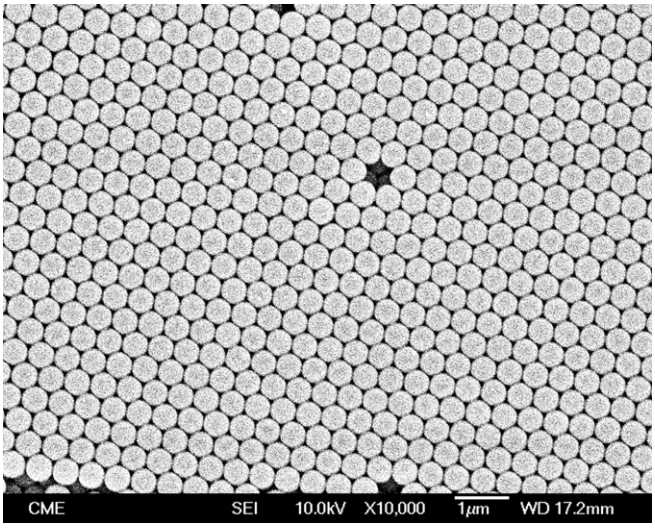

Fig. 1. SEM image of PS-MAA particles (sample 2).

The DCP values of the particle sizes are larger than the SEM estimates, since they correspond to the particle hydrodynamic size in the suspension and to dried particle size, respectively [20]. The ratio between both parameters increases with MAA content in the particles. The presence of MAA monomers at the particle surface increases the hydrodynamic radius by hydrophilic interactions with water molecules. Some positive deviation of the hydrodynamic diameter could be expected due to the uncertainty of the PS-MAA particle density (for all particles we have considered the styrene bulk density, 1.05 g/cm^3 [21]). The analysis of DCP measurements implies the calculation of the particle diameter d from the Stokes law. According this relation d^2 is proportional to $(\Delta\rho)^{-1}$, where $\Delta\rho$ is the difference of the particle density and the fluid density. An estimation of the error introduced in the analysis by using a constant particle density, leads to a positive deviation of 7% on the particle diameter for the maximum MAA loading of 7.4 wt%. This value is lower than the observed variation on the d(DCP)/d(SEM) ratio, and supports the view that the hydrophilic shell enhances this ratio.

The particle size dispersion can be expressed by the PDI coefficient, given by the ratio PDI $= d_v/d_n$, where d_v ($d_v^3 = \sum n_i d_i^3/\sum n_i$) and d_n ($d_n = \sum n_i d_i/\sum n_i$) are the volume and number average diameters, respectively, obtained from DCP analysis. The synthesized latexes can be considered as monodisperses, since their PDI values are less than 1.05 (see Table 1). The volume fraction corresponding to particle aggregates is less than 2%.

The particle monodispersity implies that all particles must nucleate in a short period of time [22] and then grow at the same rate. The nucleation process occurs homogenously when the aqueous phase is saturated of charged oligomers. On the other hand the partition coefficient of the MAA monomers in the styrene and aqueous phase is nearly one [23], and the polymerization rate of MAA in water is several orders of magnitude larger than the polymerization rate of S [24]. For this reason the addition of the MAA monomer into the reaction feed enhances the starting polymerization rate and oligomer stability in the aqueous phase. This would generate a large number of particle seeds making the particle diameters to decrease as MAA content rises (Table 1). Fig. 3 shows the MAA effect on the specific surface of polymer particles, A_e, given in terms of the area per mass unit, and calculated for monodisperse spheres by

$$A_e = \frac{6}{\rho d} \tag{1}$$

where ρ is the particle density and d the SEM particle diameter. A_e increases monotonically with MAA wt% into the monomer feed.

Also MAA addition biases the comonomer composition of the earlier oligo-radicals to MAA richer compositions increasing both the oligo-radical and the particle surface hydrophilicity. These hydrophilic end chains could parcel out the surface into hydrophobic plots connected/separated by hydrophilic walls.

The measured electrophoretic mobility, u, of the synthesized latexes is similar (Table 1), independently of the MAA content. The electrophoretic mobility of charged spheres can be related with the zeta potential ζ, through the Henry equation [25]:

$$u = C(\kappa R)\frac{\varepsilon\zeta}{\eta} \tag{2}$$

where ε and η are the solvent dielectric constant and viscosity respectively, and C is a function that depends on the reduced particle radius, κR, where κ is the reciprocal of the screening length. In the experimental conditions used in this work, all samples have κR values in a range of 12–27, and so the C function can be considered constant [26] (*c.a.* 2/3) in this range. As the electrophoretic mobility is similar, all latexes show analogous electrical potentials at the slipping plane (Equation (2)). Studies of PS-Acrylic acids latexes showed that the carboxylic groups of charged particle surfaces had very low effective dissociation equilibrium constants [27–29]. Hence, the main origin of the surface electrical charges must be the presence of sulphate anions originated during the polymerization process. The surface charge density at the slipping

Table 1
Monomer feed composition, polymerization yield %, SEM and DCP diameters, polydispersity index (PDI), electrophoretic particle mobility (u), zeta potential (ζ), estimated surface charge densities (σ^*) and critical coagulation concentration (*ccc*).

Sample	1	2	3	4	5
wt% MAA/monomer	0	0.5	1.4	3.2	7.4
Polymerization yield%	83	87	90	91	94
SEM d_n (nm)	545	480	390	308	235
DCP d_n (nm)[a]	564(16)	516(15)	426(13)	350(38)	284(24)
DCP d_v (nm)[a]	567(17)	517(15)	427(13)	354(40)	285(25)
PDI	1.005	1.002	1.002	1.012	1.003
d_n(DCP)/d_n(SEM)	1.04	1.07	1.09	1.15	1.21
$-u$(10^{-8} m^2 V^{-1} s^{-1})[a]	4.4(0.6)	3.8(0.3)	4.1(0.4)	4.0(0.2)	3.6(0.4)
$-\zeta$ (mV)[b]	56	49	52	51	46
$-\sigma^*$ (μC cm^{-2})	0.59	0.51	0.55	0.54	0.48
ccc (M, 0.25 wt% latex)	0.15	0.093	0.093	0.080	0.070
ccc (M, 0.05 wt% latex)	0.15	0.11	0.11	0.087	0.080

[a] Errors obtained from the corresponding standard deviation in parenthesis.
[b] Values obtained from Helmholtz–Smoluchowski equation [25].

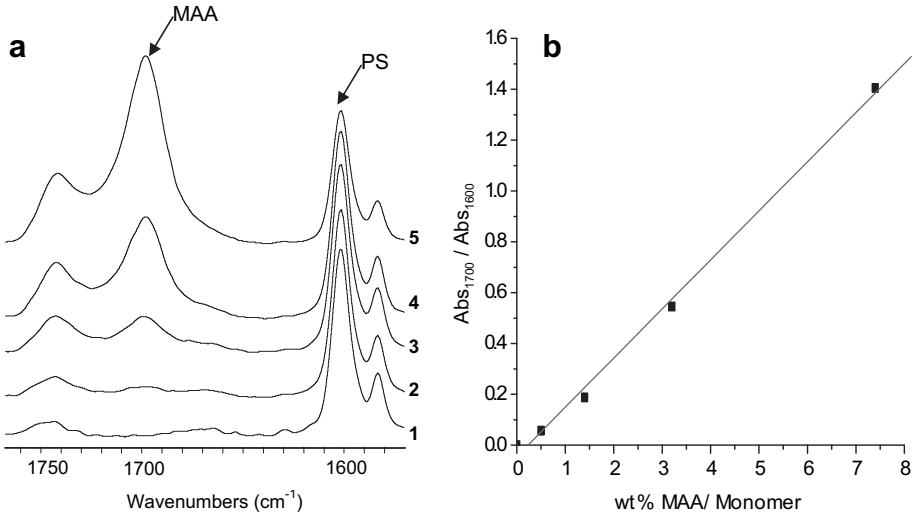

Fig. 2. a) FTIR spectra of studied samples showing the bands used to establish the correlation between relative absorbance and MAA loading in the monomer feed (b).

plane, σ^*, can be expressed in terms of the zeta potential by the following equation [25]:

$$\sigma^* = \frac{\eta\, u}{C(\kappa R)R}(1+\kappa R) \tag{3}$$

Replacing the numerical values of the known parameters in Equation (3), the surface charge density of these latexes is $\sigma^*(\mu C cm^{-2}) \approx 0.134\ u(10^{-8}\ m^2\ V^{-1}\ s^{-1})$. The charge densities at the slipping plane are obtained for all latexes (Table 1). The addition of MAA co-monomer does not increases the surface charge of these latexes.

Furthermore, it seems important to establish if the introduction of random distribution of hydrophilic carboxylic groups into the particle surfaces could enhance the latex stability against electrolytes. It has been observed that the addition of NaCl electrolyte to the suspensions screens the repulsive electrostatic interactions between particles, which form large flocks and sediment at the vial bottom, from a critical coagulation concentration (*ccc*). The *ccc* values show similar dependence with the MAA mass percentage for both considered suspension concentrations (Table 1). The bare PS particles are more stable against electrolyte coagulation that the composite PS-MAA particles. The introduction of MAA reduces the effective charge at the particle surfaces, which is also reflected in the observed changes of the electrophoretic mobilities (Table 1).

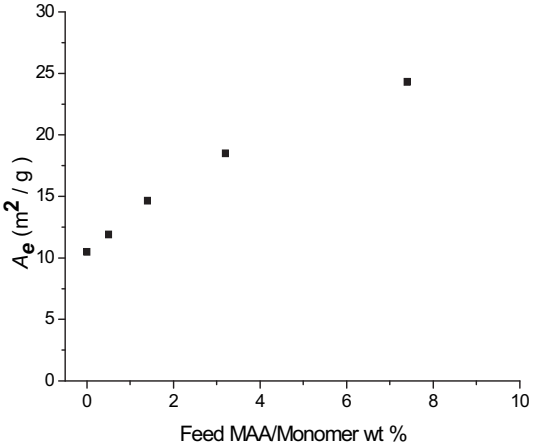

Fig. 3. Specific area of PS-MAA latexes as function of the MAA concentration.

This can be explained taking into count that in the earlier stages of polymerization, some amount of MAA monomer reacts with KPS initiator giving chains which are not incorporated into the particles; as a consequence, the number of sulphate groups present in the PS-MAA particles is reduced. Otewill [30] has demonstrated that *ccc* values are proportional to ζ^4. From this relationship the *ccc* ratio of latex 5 to latex 1 should be 0.48, which agrees with the 0.5 observed value (Table 1). Since the PS-MAA particles show less stability against the salt addition, we preclude any steric stabilization produced by MAA at the particle surfaces.

3.2. PPy coated PS-MAA latexes

Elemental analysis of nitrogen content allows determining the actual PPy/latex weight % (see Table 2). PPy polymerization efficiency was higher than 81% in all the experiments with the exception of sample 2/C (75%). At low PPy loadings the colloidal suspension is stable. No segregated PPy subphase is observed. However at high PPy loadings, particle aggregation occurs because of the screening of interparticle electrostatic repulsion in the highly ionic reaction medium [16], and also by the enhancement of the interparticle attractive London forces produced by the PPy coating. PPy grains could appear at the particle contact regions, where it is expected to find large amounts of adsorbed Py monomer and Fe^{3+} ions.

Table 2
Nitrogen content, PPy loading and conductivity of the PPy/PS-MAA composites.

Sample	N wt%	PPy wt%	σ (S cm^{-1})
1/A	1.35	6.8	0.79
2/A	1.34	6.7	0.89
3/A	1.55	7.9	0.40
4/A	1.48	7.5	0.11
5/A	1.35	6.8	2×10^{-3}
1/B	2.9	16	6.8
2/B	2.39	13	5.2
3/B	2.87	16	5.2
4/B	2.72	15	1.9
5/B	2.76	15	0.85
1/C	3.55	21	6.8
2/C	3.21	18	3.6
3/C	3.71	22	5.8
4/C	3.65	21	1.9
5/C	3.62	21	0.84

3.3. Shell morphology

The morphology of PPy/PS-MAA particles greatly depends on the composite MAA content. As an example, SEM pictures of samples 1/B, 2/B, 4/B and 5/B are shown in Fig. 4. Uniform and homogeneous PPy coatings are observed in the samples without or with very low MAA content (Fig. 4a). However, PPy grows in irregularly distributed nodules as the MAA amount increases (Fig. 4b–d). The morphology dependence on PPy content is illustrated in Fig. 5 where SEM of samples 3/A, 3/B and 3/C are depicted. The biggest difference is observed between sample 3/A, with a PPy content about 8% (Fig. 5a) that presents some "fissures" in PPy coating (in agreement with a PPy growth in localized domains), and sample 3/B with twice PPy amount (Fig. 5b) and where the whole latex surface is PPy covered. These facts suggest that, when the MAA is present, PPy growth is inhibited in the nearby of the hydrophilic walls and emerges as islands on the hydrophobic domains of the particle surface. As the PPy content increases, the hydrophilic surface regions are surmounted, and a lateral growth of the PPy grains allows a full coating of the PS-MAA (Fig. 5b). A further increment of the PPy content (Fig. 5c) enhances the PPy growth in a perpendicular direction to the latex surface, which raises the PPy overlayer thickness and PPy grain size.

Lu et al. [16] observed a similar PPy granular growth behavior on PS-poly(ethylene glycol) monomethacrylate particles, although they suggested the hydrophilic comonomer chains as the locus of the PPy polymerization.

3.4. PPy void spheres

Fig. 6 shows some examples of PPy void spheres obtained by solving the latex template in THF. Different levels of roughness are observed in the shells of the PPy voids. This granular morphology should produce a porous PPy shell. The average PPy void sizes and shell thicknesses determined from these pictures for some representative samples are summarized in Table 3. Values between 12 nm for sample 1/A and 30 nm for 5/C were found. Mechanical stability increases with PPy thickness. At large loadings the cross-linked PPy produces the stabilization of PPy sphere, independent of the particle size.

The THF treatment of the PPy/PS-MAA composites produces a diameter reduction of the voids spheres, of 12–19% (Table 2). This contraction is general in macroporous materials obtained by removal of latex templates [17,27].

For the same latex, the PPy thickness mostly increases with the loading as it is expected. On the contrary, when the PPy mass is constant, the shell thickness increases with the latex specific area per unit mass A_e (Equation (1)) unlike what would be expected if a uniform PPy coating was produced. A similar variation was observed by Lu et al. [16]. The large PPy thickness over the small particles should be correlated with the observed PPy granular growth. In this sense, from the corresponding latex diameter d, and PPy thickness x, the PPy shell density ρ_s can be calculated from Equation (4):

$$\rho_s = \frac{M_{PPy}\rho_{PS-MAA}}{M_{PS-MAA}} \frac{d^3}{\left((d+2x)^3 - d^3\right)} \tag{4}$$

where M_{PPy} is the mass PPy coating, $M_{PS\text{-}MAA}$ is the solid content of the PS-MAA suspension and $\rho_{PS\text{-}MAA}$ is the corresponding PS-MAA density. ρ_s is calculated by the ratio of the mass of PPy coating per particle and the volume of a spherical crown of diameter d and thickness x. For all the shells, calculated ρ_s is lower than 1.46 g cm^{-3}

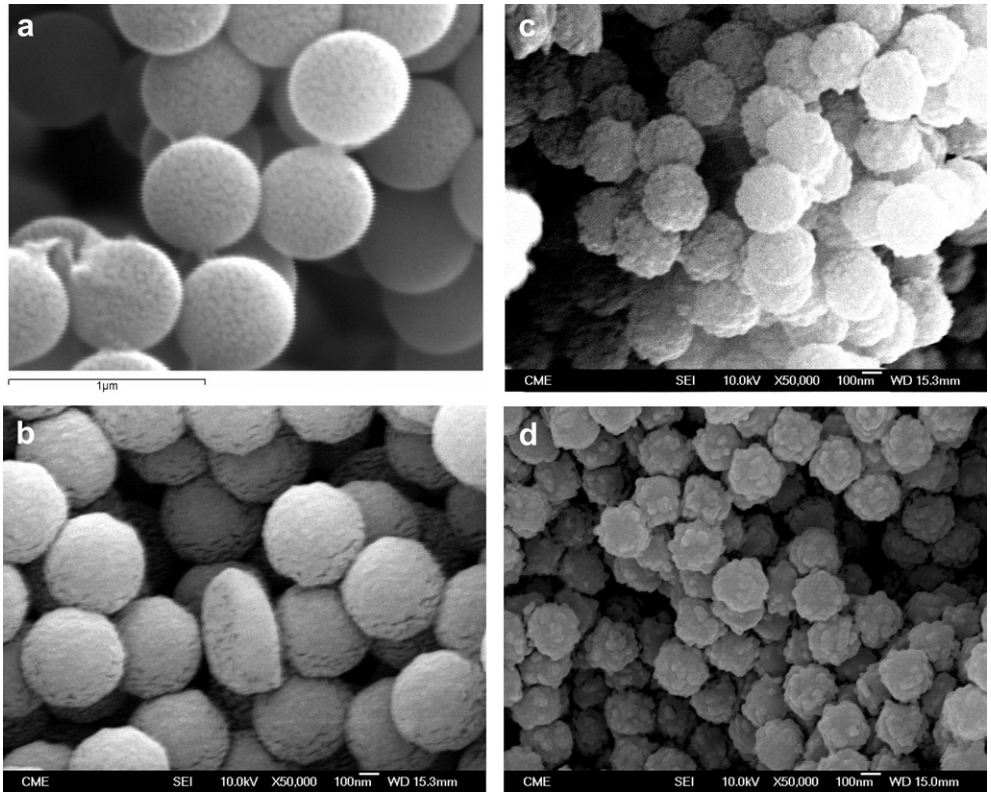

Fig. 4. SEM pictures of samples: 1/B (a), 2/B (b), 4/B (c) and 5/B (d).

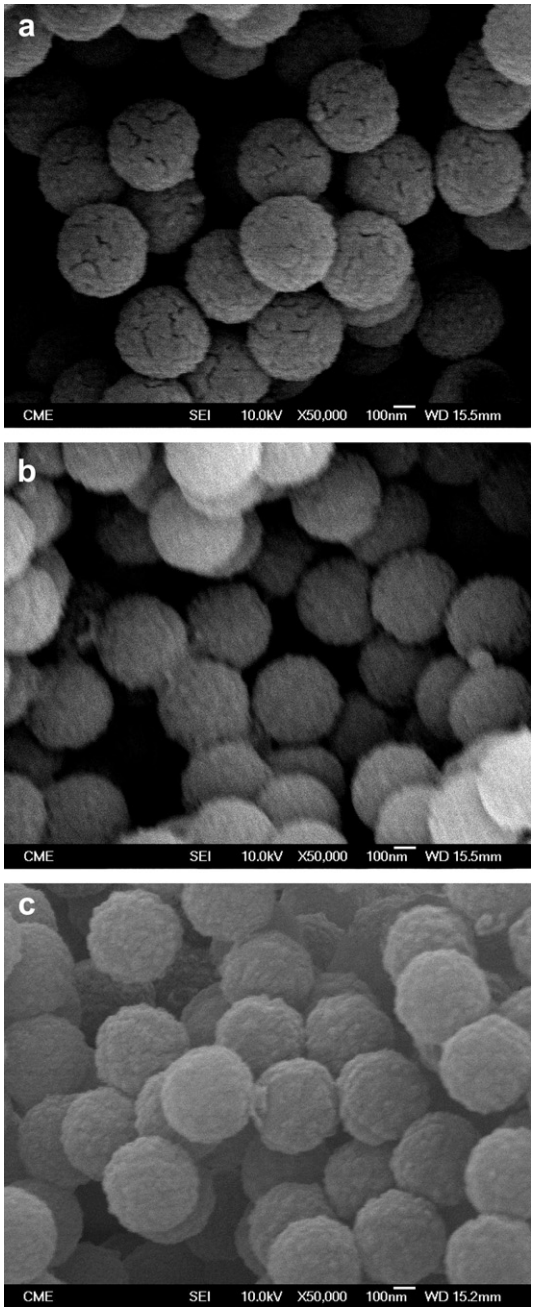

Fig. 5. SEM of samples: 3/A (a), 3/B (b) and 3/C (c).

(PPy bulk density [9]) showing the existence of PPy shell porosity. This density diminishes when the particle diameter is reduced at constant PPy mass (1A and 5A) and increases with PPy mass at constant latex diameter (Table 3). So, samples with high MAA content (samples 5) have the highest porosity as their low ρ_s values show.

3.5. Infrared spectra

PPy deposition onto PS-MAA particles was followed by infrared spectra. FTIR spectra of doped PPy coated samples show a strong absorption above 1600 cm^{-1} characteristic of conducting polymers and attributed to the free charge carriers absorption [31]. Fig. 7 displays the FTIR spectra of PS-MAA (sample 3) (a), PPy/PS-MAA (sample 3/A) (b) and the difference between (a) and (b) spectra (c). The latter exhibits all the PPy characteristic bands [32,33]: the broad absorption above 1600 cm^{-1} and bands at 1540 cm^{-1}, assigned to a combination of ν (C=C) and ν (C–C) ring stretching vibrations, 1450 cm^{-1} due to ν (C–N) stretching (overlapped by the bands ascribed to polystyrene C–H bending vibrations), 1307 cm^{-1} (C–H and N–H in plane deformations), 1090 and 1040 cm^{-1} (Py ring deformations), and 895 and 788 cm^{-1} (out of plane C–H bendings) in addition to bipolaron bands [32] at about 1170 and 964 cm^{-1}. No signals of PPy degradation is observed as no carbonyl group bands appear in the spectra.

In all the studied samples the PS-MAA content is much greater than that of PPy but the IR bands ascribable to PPy vibrations are always more intense than expected at the relatively low amounts of conducting polymer present. The same effect in the IR spectra of PPy coated poly(N-vinylpyrrolidone) stabilized PS was observed by Lascelles and Armes [9] who also reported the lack of any band attributable to the underlying latex in Raman spectra of the same PPy/latex compound [10]. These authors suggested that the core-shell morphology of the compounds would be responsible for the anomalous intensity enhancement of conducting polymer bands.

Spectra of samples with increasing amount of MAA and with different PPy loading are shown in Fig. 8. Bands ascribed to PPy C=C, C–C and to C–N stretching vibrations and to C–H and N–H in plane deformations shift to lower wavenumbers with the PPy content in the latexes (see spectrum 5/A and 5/C). This wavenumbers shift reflects the increasing PPy interactions with packing density of PPy coating. For the same reason these band wavenumbers rise with the MAA content because PPy packing diminishes in this case (see spectrum 1/B and 5/B). On the other hand, C=O stretching bands corresponding to the MAA moieties appear at the same frequency in the bare latexes and in those PPy coated indicating that PPy–latex interaction does not occur between PPy and carboxylate groups ruling out MAA as dopant and supporting the assumption of the PPy growing on the hydrophobic PS part.

3.6. Conductivity measurements

Experimental DC conductivity values, σ, measured for PPy/PS-MAA pellets are listed in Table 2. Values run between 6.8 S cm^{-1} for samples 1/B and 1/C (high PPy loading on PS substrate without MAA) and 2×10^{-3} S cm^{-1} for sample 5/A (the highest MAA content and the lowest PPy loading). An inverse relationship between conductivities, σ, and MAA concentration in the latex core is clear in these samples. Comparison of conductivity values measured for samples containing the same MAA amount but different PPy loadings shows a great increase from series A (~8%PPy) to series B (~16% PPy). A new increment in PPy loading from series B to series C does not cause a proportional rise of conductivity. This trend in the conductivity to saturate (σ_s) at high polymer loading is a general behavior observed in polypyrrole coated latexes [9,13,16].

The dependence of the composite conductivity on the PPy loading mass per latex unit area, $\Gamma = w/100A_e$, is presented in Fig. 9 in a log σ versus Γ plot, where w is the actual PPy/latex wt% given in Table 2, and A_e is given by Equation (1). The conductivity behavior of PPy/PS-MAA latexes (Series A and B) is described by a master curve in terms of Γ. As the PPy content in Series C is higher than that corresponding to saturation conductivity, σ values for Series C shift to higher Γ. A three order of magnitude change in conductivity is observed when Γ goes from 0.25×10^{-6} g cm^{-2} to 1.5×10^{-6} g cm^{-2}. This corresponds to a typical percolative behavior where a conducting network emerged at a critical value of PPy surface mass loading Γ_c. As a consequence σ in PPy/PS-MAA samples can be described by a percolation scaling law:

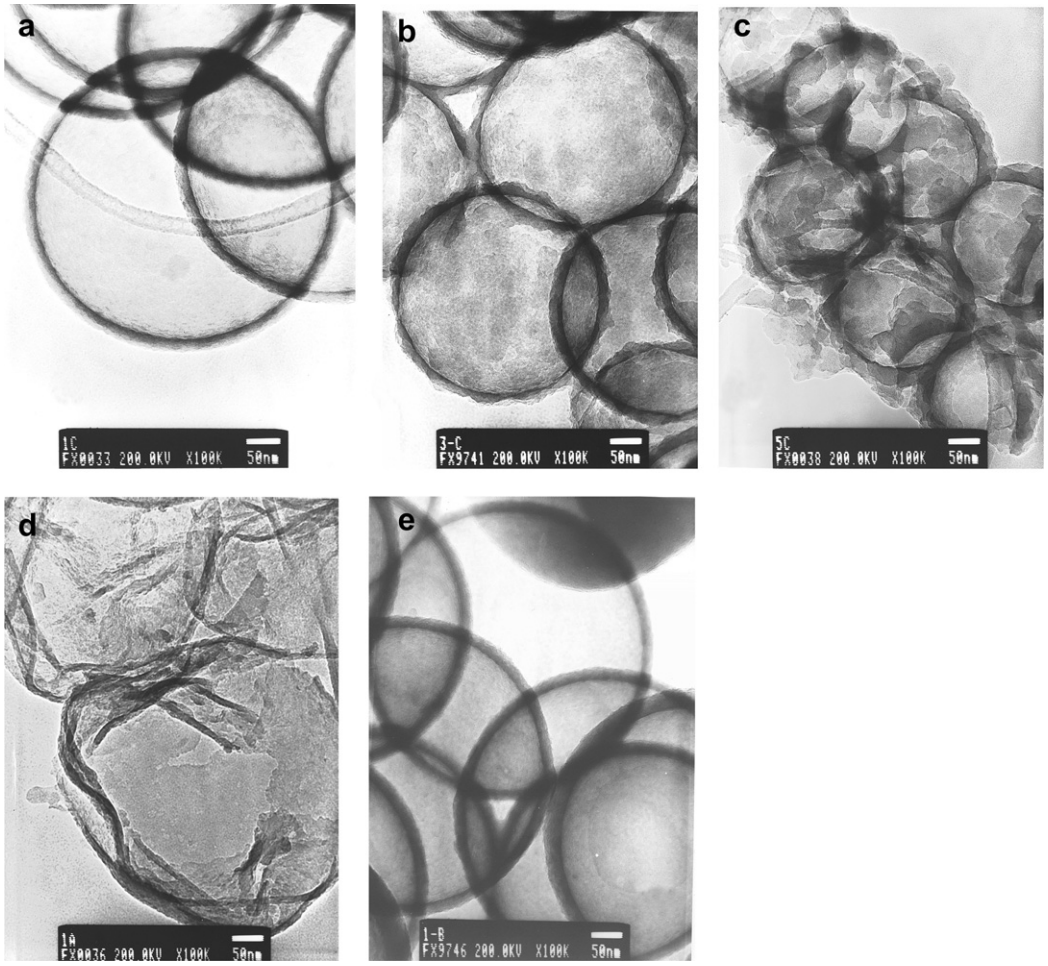

Fig. 6. TEM of PPy void spheres for samples: 1/C (a), 3/C (b), 5/C (c), 1/A (d) and 1/B (e).

$$\sigma = a(\Gamma - \Gamma_c)^t \quad (5)$$

where $a = \frac{\sigma_s}{(\Gamma_s - \Gamma_c)^t}$ is a constant, which can be expressed by the ratio of the saturation conductivity, σ_s, and the coating range where the scaling law is followed $\Gamma_c < \Gamma < \Gamma_s$, being Γ_s the saturation coating loading. The theoretical value of the critical exponent t calculated for 3D systems of random resistor lattices [34–36] is near 2. However, confirmation of this value is found only in a limited number of experiments in real disordered systems [37]. The application of percolation theory (Equation (5)) to the master curve data (Series A and B) allows to determine both critical parameters Γ_s and t for these PPy/PS-MAA composites. For a given Γ_s value, the critical exponent was obtained by a least square fitting of the logarithmic expression of Equation (5). This procedure was repeated by varying Γ_c, and a series of correlation coefficients r are obtained. The maximum value of r defined the optimal t and Γ_c parameters [35]. The PPy/PS-MAA fitted parameters are shown in Table 4. The parameters obtained for PPy coated PS [9] and PPy coated polybutylmethacrylate [13] are also included in Table 4 for comparison. In these systems the PPy coating process was performed after stabilizing the templates with PVP.

All analyzed coated latexes follow the scaling law given by Equation (5) with t exponents near the theoretical value of 2. This indicates that electron conduction occurs in a 3D network through

Table 3
Number average diameter of PPy/PS-MAA composites $d_{PPy/PS\text{-}MAA}$, and of the PPy voids d_{PPy}, average PPy thickness x, and PPy shell density ρ_s.

Sample	$d_{PPy/PS\text{-}MAA}$(nm) *SEM*	d_{PPy}(nm) TEM	x (nm) TEM	ρ_s(g cm^{-3})
1/A	550	+	12	0.56
1/B	575	495	25	0.66
1/C	612	495	21	1.12
5/A	270	236	19	0.13
5/B	285	+	25	0.23
5/C	275	250	30	0.285

+ Broken spheres.

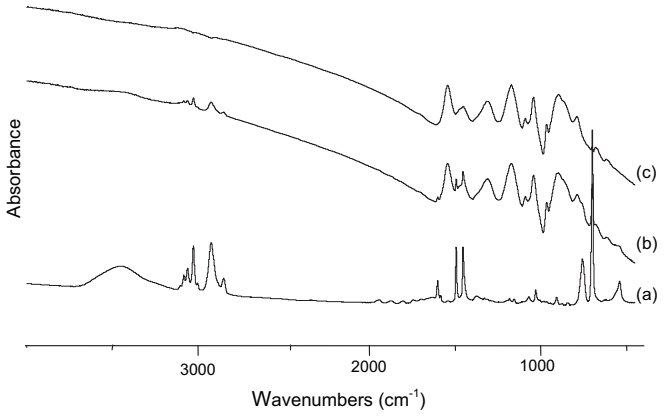

Fig. 7. FTIR spectra of PS-MAA (sample 3) (a); PPy/PS-MAA (sample 3/A) (b); difference spectrum (c).

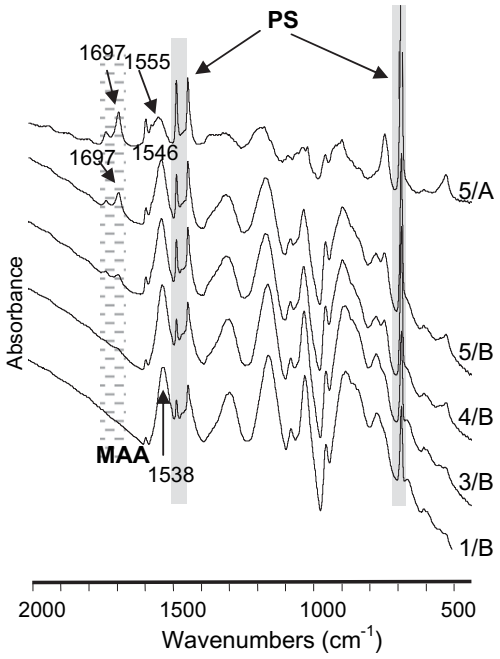

Fig. 8. FTIR spectra of PPy/latex samples (series B). PS and MAA absorption regions are marked in the figure.

the particle surface contacts. We note that each system shows different surface loading threshold, Γ_c, and proportionality constant, a, being both parameters mainly determined by the PPy shell morphology. PPy/PS-PVP and PPy/PS-MAA latexes have similar Γ_c values; however at the same PPy loading the conductivities of PPy/PS-PVP materials are lower. PPy/PBMA-PVP latexes [13] show a threshold surface loading almost three times larger than PPy/PS samples, which must be due to the more patchy structure observed in these coatings. Since the $(\Gamma_s - \Gamma_c)$ range is similar in all latexes, the large differences observed in the proportionality constant (a) would be ascribed to variations in the conductivity saturation at large PPy loadings. As it is observed in Fig. 8, the saturation conductivity σ_s, of PPy/PS-MAA master curve is near 7 S cm^{-1}, and it is achieved for the most hydrophobic template, at coatings Γ_s around 1.5 $\times$ 10^{-6} g cm^{-2}, which corresponds to a 16 wt% PPy loading. This conductivity is the maximum conductivity value reported for bulk chloride doped PPy [38].

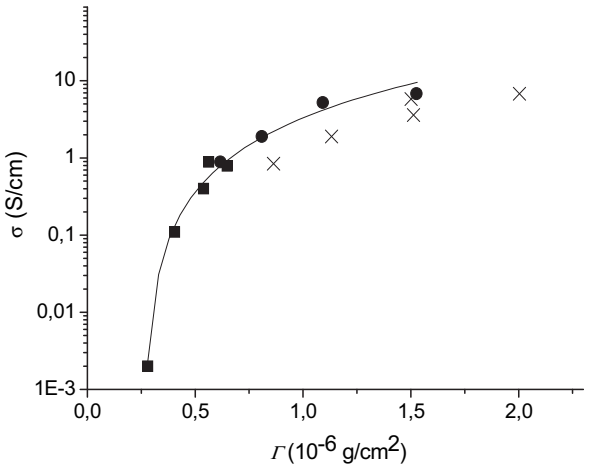

Fig. 9. Sample conductivity against PPy mass surface loading for series A (■); series B (•); series C (×).

Table 4
Fitted parameters of the conductivity power law Equation (5) in its logarithm form for several PPy/latex composites.

System	d(nm)	t	Γ_c (10^{-6} g cm^{-2})	Ln a	r
PPy/PS-PVP [9]	1800	1.99(0.06)	0.314(0.005)	−0.7(0.2)	0.998
PPy/PBMA-PVP [13]	995	2.0(0.06)	0.76 (0.04)	−5.3(0.2)	0.98
PPy/PS-MAA (this work)	200–600	1.98(0.07)	0.262(0.002)	1.8(0.1)	0.995

Errors obtained from the corresponding standard deviation of the fitted parameters in parenthesis.

Lascelles et al. [9] reported a conductivity of 6 S cm^{-1} for 1.57 μm PPy coated PS-PVP latexes at 18.4 wt% PPy loading ($\Gamma \cong 5 \times 10^{-6}$gcm^{-2}). Conductivity values from reference [9] follow the same conductivity percolation law with a slightly lower threshold value but the PPy loading per latex surface area needed to obtain the same composite conductivity is much larger. Probably this is a consequence of the PVP stabilizer resistivity.

The saturation conductivity in PPy/PBMA-PVP composites [13] is lower than in PPy/PS composites as a consequence of the different chemical composition of the latex surfaces with a higher hydrophilic character.

It is also worth to mention that the PPy coating of PS-MAA latexes produces a strong reduction of the electrical conductivity threshold from 18 wt% reported for PPy/PS blends [39] to 6.3 and 2.7 PPy wt% for our samples 5 and 1, respectively. This large reduction of the percolation threshold is a consequence of the PPy confinement at the latex surfaces.

4. Conclusions

In this work core-shell particles of PPy/PS-MAA have been obtained by chemical polymerization of pyrrole in monodisperse PS-MAA latexes. $FeCl_3$ was used as oxidant and reaction yields higher than 75% were obtained. The template sizes and surface chemical composition can be controlled by varying the MAA amount present in the monomer feed. Thin PPy shells with thickness between 25 and 12 nm are achieved. Uniform and high packed coatings are observed in SEM pictures of samples with no MAA content. Furthermore, when MAA wt% rises, low packed PPy nodules constitute the shells.

The PPy/latex composites follow a three-dimensional percolation model of the conductivity, as the fitted power matches the theoretical value of 2. For bare styrene particles saturation conductivity is observed near 7 S cm^{-1} at PPy mass surface densities around 1.5 $\times$ 10^{-6} g cm^{-2}. To achieve high saturation conductivities of these composites it is important to enhance the PPy interaction with the particle surface, which controls the PPy grain size, the insulating regions of the coatings and finally the PPy overlayer porosity.

Acknowledgements

The authors thank to the Ministerio de Educación y Ciencia (Spain), and to UCM/Banco Santander program for financial support under Projects: MAT-2007-65711-C04-02 and GR58/08-921556 respectively. M.P. thanks the Ministerio de Educación y Ciencia (Spain) for a research contract. Technical assistance from the Microscopy Centre (UCM) and the Elemental Analysis Service (UCM) are acknowledged. We thank Dr. Fernando Bresme for insightful comments.

References

[1] Skotheim TA, Elsenbaumer RL, Reynolds JR, editors. Handbook of conducting polymers. New York-Basel: Marcel Dekker Inc; 1998.
[2] Diaz AF, Kanazawa KK, Gardini G. J Chem Soc Chem Commun 1979;14:635–6.
[3] Myers RE. J Electron Mater 1986;15:61–9.
[4] Jasne SJ, Chiklis CK. Synth Met 1986;15:175–82.
[5] Duport M, Levassort C, Olmedo L. Synth Met 1991;43:3063–6.
[6] Wiersma AF, Steeg LMA, Jongeling TJM. Synth Met 1995;71:2269–70.
[7] Lascelles SF, Armes SP. Adv Mater 1995;7:864–6.
[8] Perruchot C, Chehimi MM, Delamar M, Lascelles SF, Armes SP. Langmuir 1996;12:3245–51.
[9] Lascelles SF, Armes SP. J Mater Chem 1997;7:1339–47.
[10] Lascelles SF, Armes SP, Zhdan PA, Greaves SJ, Brown AM, Watts JF, et al. J Mater Chem 1997;7:1349–55.
[11] Cairns DB, Armes SP. Langmuir 1999;15:8052–8.
[12] Lu Y, Pich A, Adler H. Synth Met 2003;135–136:37–8.
[13] Cairns DB, Khan MA, Perruchot C, Riede A, Armes SP. Chem Mater 2003;15:233–9.
[14] Cho SH, Kim WY, Jeong GK, Lee YS. Colloids Surf A Physicochem Eng Asp 2005;255:79–83.
[15] Ormond-Prout J, Dupin D, Armes SP, Foster NJ, Burchell MJ. J Mater Chem 2009;19:1433–42.
[16] Lu Y, Pich A, Adler HJP, Wang G, Rais D, Nespurek S. Polymer 2008;49:5002–12.
[17] Carbajo MC, Gómez A, Torralvo MJ, Enciso E. J Mater Chem 2002;12:2740–6.
[18] Carbajo MC, Climent E, Enciso E, Torralvo MJ. J Colloid Interface Sci 2005;284:639–45.
[19] Armes SP, Miller JF, Vincent B. J Colloid Interface Sci 1987;118:410–6.
[20] Pich A, Lu Y, Adler H. J Colloid Polym Sci 2003;281:907–15.
[21] Brandrup J, Immergut EH, Grulke EA, editors. Polymer handbook. 4th ed. New York: John Wiley and Sons; 2003.
[22] LaMer VK, Dinegar RH. J Am Chem Soc 1950;72:4847–54.
[23] Vijayendran BR. J Appl Polym Sci 1979;23:893–901.
[24] Shoaf GL, Poehlein GW. J Appl Polym Sci 1991;42:1213–37.
[25] Hiemenz P, Rajagopalan R. Principles of colloid and surface chemistry. New York: Marcel Dekker; 1997.
[26] Wiersema PH, Loeb AL, Overbeek JTG. J Colloid Interface Sci 1966;22:78–99.
[27] Carbajo MC., Ph. D. Thesis, Madrid. Universidad Complutense, 2004.
[28] Quesada-Pérez M, Callejas-Fernández J, Hidalgo-Álvarez R. J Colloid Interface Sci 1998;206:354–6.
[29] Gisler T, Schulz SF, Borkovec M, Sticher H, Schurtenberger P, D'Aguanno B, et al. Chem Phys 1994;101:9924–36.
[30] Ottewill RH. In: Lovell PA, El-Aasser MS, editors. Emulsion polymerization and emulsion polymers. Chichester: Wiley; 1997. p. 75.
[31] Lei J, Liang W, Martin CR. Synth Met 1992;48:301–12.
[32] Tian B, Zerbi G. J Chem Phys 1990;92:3886–98.
[33] Elyashevich K, Rosova EY, Sidorovich AV, Kuryndin IS, Trchová M, Stejskal J. Eur Polym J 2003;39:647–54.
[34] Gingold DB, Lobb C. J Phys Rev B 1990;42:8220–4.
[35] Yoshida K. J Phys Soc Jpn 1990;59:4087–95.
[36] Clerc JP, Podolskiy VA, Sarychev AK. Eur Phys JB 2000;15:507–16.
[37] Vionnet-Menot S, Grimaldi C, Maeder T, Strassler S, Ryser P. Phys Rev B 2005;71. 064201-1-12.
[38] Armes SP. Synth Metals 1987;20:365–71.
[39] Wang HL, Toppare L, Fernández JE. Macromolecules 1990;23:1053–9.